ACS APPLIED MATERIALS & INTERFACES

Research Article

www.acsami.org

Photocurrent Enhanced by Singlet Fission in a Dye-Sensitized Solar Cell

Joel N. Schrauben,[†] Yixin Zhao,[†] Candy Mercado,[†,‡] Paul I. Dron,[‡] Joseph L. Ryerson,[†,‡] Josef Michl,[‡,§] Kai Zhu,*[,†] and Justin C. Johnson*[,†]

[†]National Renewable Energy Laboratory, 15013 Denver West Parkway, Golden, Colorado 80401, United States

[‡]Department of Chemistry and Biochemistry, 215 UCB, University of Colorado, Boulder, Colorado 80309, United States

[§]Institute of Organic Chemistry and Biochemistry, Academy of Sciences of the Czech Republic, Flemingovo nam. 2, 16110 Prague, Czech Republic

Supporting Information

ABSTRACT: Investigations of singlet fission have accelerated recently because of its potential utility in solar photoconversion, although only a few reports definitively identify the role of singlet fission in a complete solar cell. Evidence of the influence of singlet fission in a dye-sensitized solar cell using 1,3-diphenylisobenzofuran (DPIBF, **1**) as the sensitizer is reported here. Self-assembly of the blue-absorbing **1** with co-adsorbed oxidation products on mesoporous TiO_2 yields a cell with a peak internal quantum efficiency of ∼70% and a power conversion efficiency of ∼1.1%. Introducing a ZrO_2 spacer layer of thickness varying from 2 to 20 Å modulates the short-circuit photocurrent such that it is initially reduced as thickness increases but **1** with 10−15 Å of added ZrO_2. This rise can be explained as being due to a reduced rate of injection of electrons from the S_1 state of **1** such that singlet fission, known to occur with a 30 ps time constant in polycrystalline films, has the opportunity to proceed efficiently and produce two T_1 states per absorbed photon that can subsequently inject electrons into TiO_2. Transient spectroscopy and kinetic simulations confirm this novel mode of dye-sensitized solar cell operation and its potential utility for enhanced solar photoconversion.

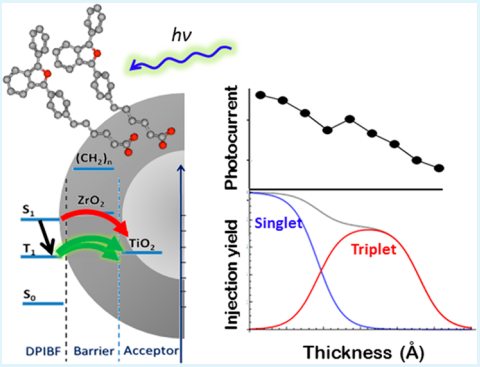

KEYWORDS: *photovoltaics, singlet fission, triplet, spectroscopy, charge transfer, photocurrent*

INTRODUCTION

The quest for inexpensive light-harvesting systems that exceed the Shockley−Queisser limit has led many researchers to explore singlet fission (SF),[1] which is the molecular analogue of multiple-exciton generation (MEG) in semiconductors.[2] SF occurs from a photoexcited singlet state and results in two triplet excitons. From its discovery and initial characterization decades ago,[3] further understanding of SF progressed slowly until the past several years. A more complete investigation of the SF process theoretically[4−6] and experimentally[7−9] and a more comprehensive search for new SF chromophores[10−13] have reinvigorated the field that now benefits from advancements made in all aspects of the process, from fundamental to practical. The recent demonstration of a solar cell with a >100% external quantum efficiency in photocurrent was a major achievement,[14] but still, few studies report true evidence of the influence of SF in devices. It should be noted that by itself, a solar cell made of SF chromophores that populates two lowest triplet states (T_1) at half the energy of the lowest singlet state (S_1) populated after one photon absorption will not exceed the Shockley−Queisser limit. A second layer of chromophores that absorbs lower-energy solar radiation and produces one electron−hole pair per photon must be included.[15,16] Unlike the usual series-connected tandem devices, current matching is not necessary to achieve the greatest benefit from SF: if the T_1 energy of the SF chromophores and the S_1 energy of the ordinary chromophores are approximately aligned, the photocurrents are additive, and the two chromophore types can be included as mixed or separated layers, the latter because in some cases competitive dye adsorption or light absorption may be unwanted.

Conjugated organic systems hold great promise for low-cost photovoltaics,[17] but charge transport properties are rarely as favorable as those of inorganic semiconductors. However, for dye-sensitized solar cells (DSCs),[18] the issue of charge transport within the light-harvesting phase is irrelevant, and thus, DSCs serve as a unique platform for testing new and potentially revolutionary photophysical concepts for enhanced photocurrent generation without concern for poor charge transport. In addition, the aforementioned layered SF/ordinary chromophore device concept is relatively facile to produce using standard DSC fabrication methods.[19] Toward this end,

Received: September 15, 2014
Accepted: January 8, 2015
Published: January 21, 2015

DOI: 10.1021/am506329v
ACS Appl. Mater. Interfaces 2015, 7, 2286−2293

we have fabricated DSCs using the SF compound 1,3-diphenylisobenzofuran (DPIBF, **1**); we have studied its photophysics extensively.[20−22] Even without a covalent linker, **1** can successfully sensitize mesoporous TiO_2 with the assistance of co-adsorbents, producing DSCs with carrier diffusion lengths greater than 10 times the film thickness and an internal quantum efficiency (IQE) of >70%. With efficient charge transport achieved, the short-circuit photocurrent informs on the quantum yield of electron injection, which may contain contributions from injected electrons from **1** S_1 or T_1. In the latter case, SF has been shown to be the dominant mechanism for producing triplets in polycrystalline **1**, yielding 2 × T_1 from S_1 with a near unity efficiency.[23−25] However, with **1** in the proximity of the nanocrystalline acceptor, the competing process of charge injection from S_1 to TiO_2 on an ultrafast time scale changes the kinetic competition, resulting in low T_1 yields (Φ_T). To restore Φ_T, we increase the S_1 lifetime by placing a barrier between **1** and TiO_2. As a result, high Φ_T due to SF is partially restored, which is then reflected in a nonmonotonic dependence of the short-circuit photocurrent density (J_{sc}) on the barrier thickness.

RESULTS AND DISCUSSION

The mesoporous TiO_2 substrates were fabricated by screen printing from a colloidal TiO_2 paste (~20 nm in particle size) onto fluorine-doped tin oxide (FTO) glass. Typical film thicknesses were 4−8 μm. Compound **1** is relatively soluble in many common organic solvents, and several solutions were tested for staining the mesoporous TiO_2 substrates. Acetonitrile solutions were generally found to result in the best solar cell performance, although in all cases degassed solvents produced poor adsorption onto TiO_2. Some **1** did adhere to the TiO_2 during air-free staining, but after successive rinses with acetonitrile, the color faded, which indicates detachment of **1**. Air-saturated solutions of **1** were much more successful at staining the TiO_2 even when the electrolyte was added. Compound **1** is known to be unstable in oxygenated solutions[26] and can form various oxidation products (**2**−**4** in Chart 1). Compounds **2** and **4** were isolated from the mixtures and their identities confirmed by nuclear magnetic resonance (NMR) or UV−vis to be those previously reported.[26,27] With exposed carbonyl groups upon the opening of the furan ring, oxidized **1** may be more likely to adhere to the TiO_2 surface than **1**. After adhesion, binding of pristine **1** is achieved by van der Waals interactions with the oxidation products. It is also possible that **1** initially binds weakly but that the relatively insoluble oxidation products serve to encapsulate it on the TiO_2 surface, preventing detachment of the chromophores.

Photoelectrodes sensitized in this way were dark yellow in color (absorbing ~50% of 420 nm light) and remained stable for months in air. The absorption spectra contained broadened features due to scattering and a mixture of molecular species, but only **1** possesses significant absorption beyond 400 nm (Figure 1). Efforts aimed at utilizing **5**, a derivative of **1**, for covalent linking are described below.

Chart 1. Structures of Molecules Discussed in the Text

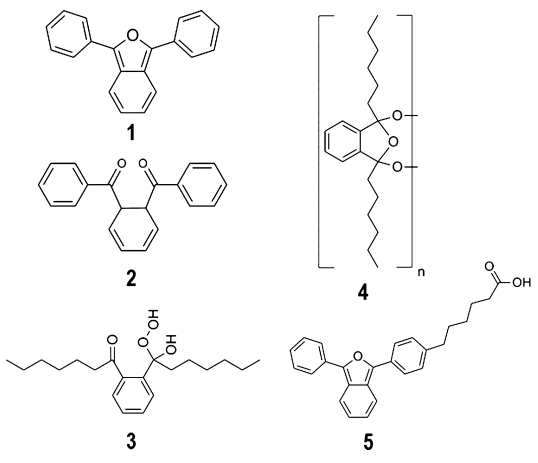

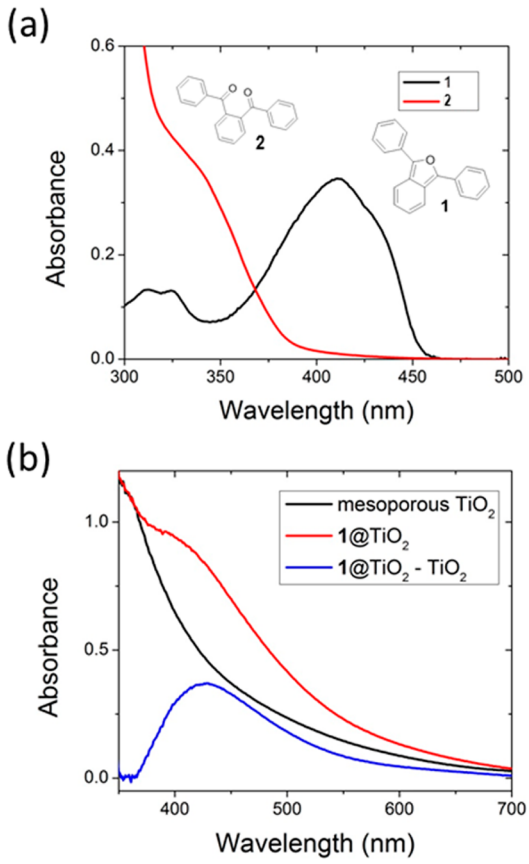

Figure 1. (a) Absorption of **1** and **2** in an acetonitrile solution. (b) Absorption of mesoporous TiO_2 substrate, **1** adsorbed to TiO_2, and the difference spectrum.

Figure 2 shows current−voltage (I−V) characteristics of DSCs made of **1** in acetonitrile at varying concentrations [electrolyte being 0.8 M HDMII (1-hexyl-2,3-dimethylimidazolium iodide) and 0.05 M I_2 in methoxypropionitrile]. The devices also contain a TiO_2 scattering layer. The best device produced a short-circuit photocurrent density of ~3.3 mA/cm^2, an open-circuit voltage of ~0.51 V, and a fill factor of ~0.7 [total power conversion efficiency (PCE) of ~1.1%]. The action spectrum [incident photon current conversion efficiency (IPCE)] (Figure 2b) shows a peak at 360 nm due to TiO_2 and a peak near 420 nm due to **1**. Extinction measurements reveal a maximal absorption of 30−50% at the absorption peak of **1**. Greater absorption is achieved for devices with a scattering layer, which increases the uncertainty in the true absorption due to **1**. Combining the IPCE and the absorbance gives a maximal internal quantum efficiency (IQE) between 60 and 70%, roughly constant across the absorption band of **1**. The tail

DOI: 10.1021/am506329v
ACS Appl. Mater. Interfaces 2015, 7, 2286−2293

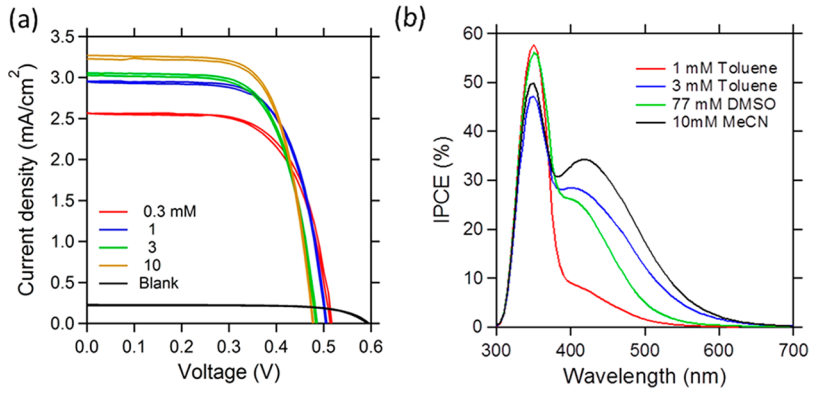

Figure 2. (a) $I-V$ curves for **1**-sensitized TiO_2 at varying sensitizer concentrations. (b) IPCE for various devices.

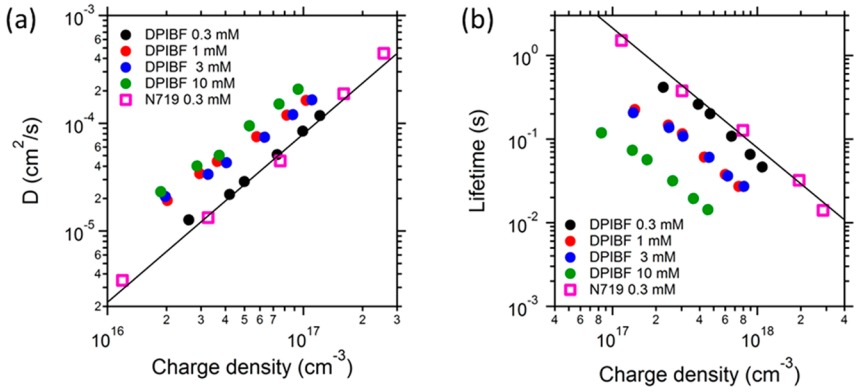

Figure 3. Comparison of **1** and N719 dyes with respect to (a) electron diffusion coefficient and (b) recombination lifetime as a function of photoexcited carrier density.

beyond 500 nm in the IPCE likely arises from aggregated **1**, which can be detected in thin film absorption. Further solar cell results can be found in Figure S1 of the Supporting Information.

Intensity-modulated photocurrent spectroscopy (IMPS) measurements allow for the determination of the charge carrier diffusion coefficient (D), while intensity-modulated photovoltage spectroscopy (IMVS) provides the charge carrier lifetime (τ).[28] Diffusion length L_D can then be calculated from the equation $L_D = (\tau D)^{1/2}$. IMPS measurements (Figure 3) of both N719- and DPIBF-sensitized mesoporous TiO_2 versus charge carrier density reveal a D of $\sim 10^{-4}$ cm^2 s^{-1} at a low concentration of **1** and an effective carrier density of 10^{17} cm^{-3}. D increases slightly for much higher concentrations of **1** in acetonitrile, presumably because of passivation of transport-limiting traps on the TiO_2 surface. In contrast, the lifetime measured from IMVS (Figure 3b) decreases for an increasing charge density for both N719 and **1** and is shorter for highly concentrated solutions. The most important factor is L_D ($\sim$120 μm), which is essentially the same for N719 and **1** at low concentrations. The lowest value ($\sim$50 μm) occurs for the most highly concentrated **1**-sensitized solutions, which is still roughly 1 order of magnitude larger than the film thickness. These results indicate that under the conditions used to sensitize photoelectrodes for solar cells, **1** does not cause significant recombination or hinder charge transport. Thus, even in the worst-case scenario, it is still expected that nearly 100% of injected carriers will be collected as photocurrent.

Figure 4 depicts the device architecture, energy levels, and rate constants for various processes occurring after photo-

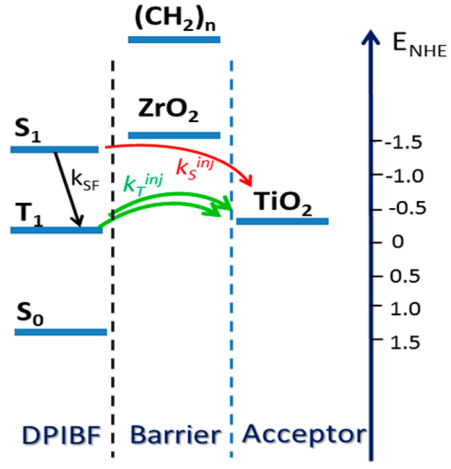

Figure 4. Schematic of interfacial charge transfer in **1**-sensitized photoelectrodes. Approximate conduction band and HOMO/LUMO energies are shown.

excitation. Because for polycrystalline **1** SF is known to proceed in $\sim$30 ps, the <1 ps injection time (*vide infra*) from S_1 almost completely inhibits any opportunity for SF followed by T_1 injection. Thus, we chose to add a zirconia spacer layer between TiO_2 and **1** to reduce the S_1 injection rate. We expect that the rate constant for injection will be reduced according to eq 1,[29]

$$k_{inj} = k_0 e^{-\beta d} \quad (1)$$

where d is the barrier width, k_0 is the rate constant at zero width, and β is the electron tunneling decay constant. If we

DOI: 10.1021/am506329v
ACS Appl. Mater. Interfaces 2015, 7, 2286−2293

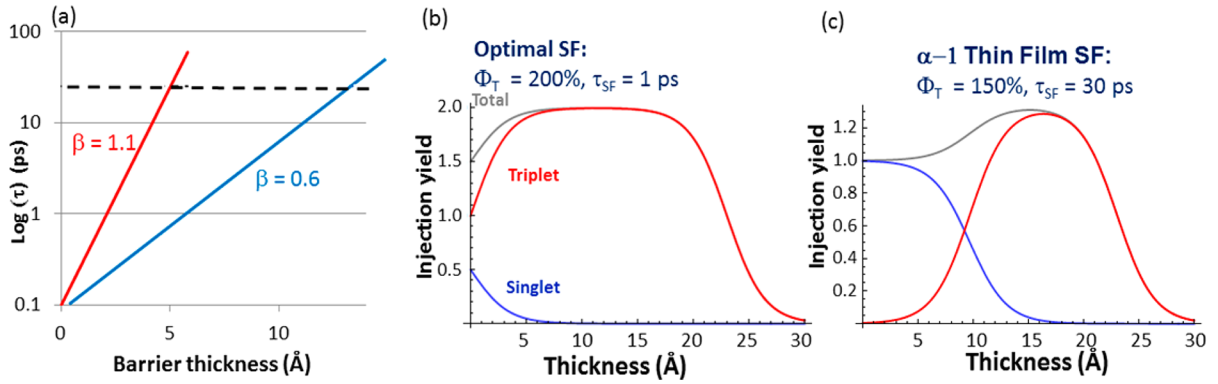

Figure 5. (a) Calculation of threshold thickness for equal rates of SF and injection from S_1. The dashed line is 30 ps, the red line for a saturated alkane barrier, and the blue line for a ZrO_2 barrier. Simulation with $\beta = 0.6$ for (b) optimal SF and (c) parameters known from thin films at room temperature.

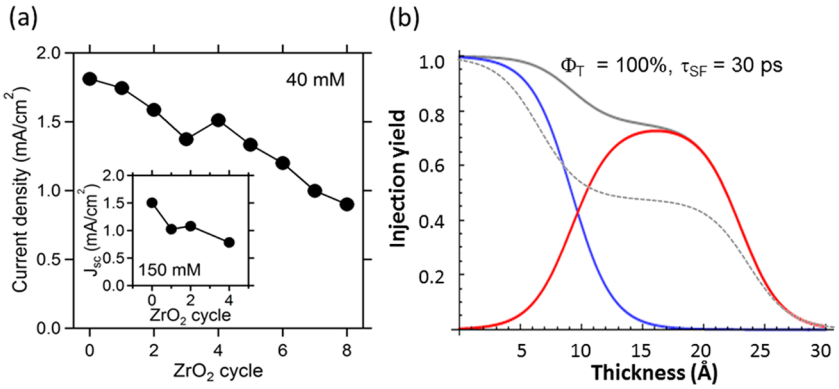

Figure 6. (a) J_{sc} vs cycle number for **1**-sensitized TiO_2/ZrO_2 films. The inset shows data at a higher concentration. (b) Injection yield predicted from kinetic simulation: blue for S_1 injection, red for T_1 injection, and gray for total. The dashed gray line shows $\Phi_T = 50\%$ and $\tau_{SF} = 5$ ps.

assume an initial injection rate constant k_{S1}^{inj} of 10 ps^{-1} at $d = 0$ and $\beta = 0.6$, the thickness at which the SF rate constant should exceed k_{S1}^{inj} is roughly 1.5 nm (Figure 5a). Predictions using a kinetic model for the photocurrent versus barrier thickness with either ZrO_2 or an aliphatic hydrocarbon barrier ($\beta = 1.1$) are shown in panels b and c of Figure 5, using both idealized parameters and those measured on thin films of **1**. The S_1 radiative lifetime and the T_1 lifetime are obtained from previous results, while the S_1 injection time at $d = 0$ is taken from ultrafast transient absorption experiments (*vide infra*). The T_1 injection time is estimated to be 1−2 orders of magnitude slower than that from S_1, consistent with studies of N719,[32] although the exact value had little effect on the photocurrent versus d curve as long as K_{T1}^{inj} was significantly larger than the T_1 decay rate constant. k_{SF} is thought to be equal to $(30\ ps)^{-1}$, which is the value measured in α-**1** films at low excitation densities. In β-**1** films that have a different morphology, k_{SF} is not accurately known but can be inferred from Φ_T to be less than $(2\ ns)^{-1}$.[23] Because interactions within the self-assembled layers on the mesoporous TiO_2 surface are likely to encompass both α-**1** and β-**1** types of morphologies, we assume that only α-**1**-type geometries can exhibit sufficiently fast SF to be relevant in the solar cells, and the low Φ_T then reflects the mixture of morphologies. Φ_T is known to be as high as 200% under certain conditions, but the value depends highly on the intermolecular geometries due to both the presence of competing pathways (e.g., excimer formation) and differing values of key SF matrix elements.[33] The T_1 injection yield is given by the red curves in panels b and c of Figure 5, while the S_1 injection yield is shown as the blue curves. The sum of the two curves is colored gray and reflects the experimentally observable photocurrent. The exact expressions for these contributions can be found in the Supporting Information.

To verify the slowed injection kinetics with a known dye, we measured electron injection times from the dye Z907 into TiO_2 through a varying thickness ZrO_2 spacer. Although the injection time without a spacer layer is much faster than our instrument response, three cycles of ZrO_2 deposition led to an injection component up to 1 order of magnitude slower (Figure S2 of the Supporting Information). The zirconia was deposited by chemical bath deposition,[30] which builds layers with thicknesses between 0.3 and 1.0 nm per cycle. The layers are conformal, but with up to 50% thickness variance. The concentration of the precursor, which varied from 0.04 to 0.15 M, directly affects the average thickness of ZrO_2. IMPS/IMVS measurements on sensitized TiO_2/ZrO_2 films showed a monotonically increasing τ and decreasing D as ZrO_2 increases but an L_D that varies little from that shown in Figure 3 and always remains >6 times the film thickness (Figure S3 of the Supporting Information).

The short-circuit photocurrent density was measured as a function of the number of zirconia deposition cycles (Figure 6) for electrodes sensitized with air-saturated solutions. For two different sets of electrodes and two different precursor concentrations, it was discovered that the photocurrent does not decrease monotonically, matching predictions from simulations. There is an initial decrease followed by a small increase around cycle 2 for a precursor concentration of 150 mM and cycle 4 for a concentration of 40 mM. The slight rise

DOI: 10.1021/am506329v
ACS Appl. Mater. Interfaces 2015, 7, 2286−2293

Scheme 1. Synthesis of 5

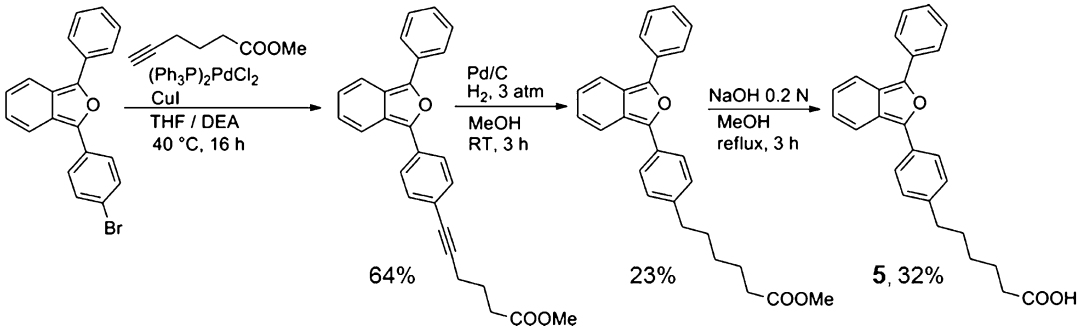

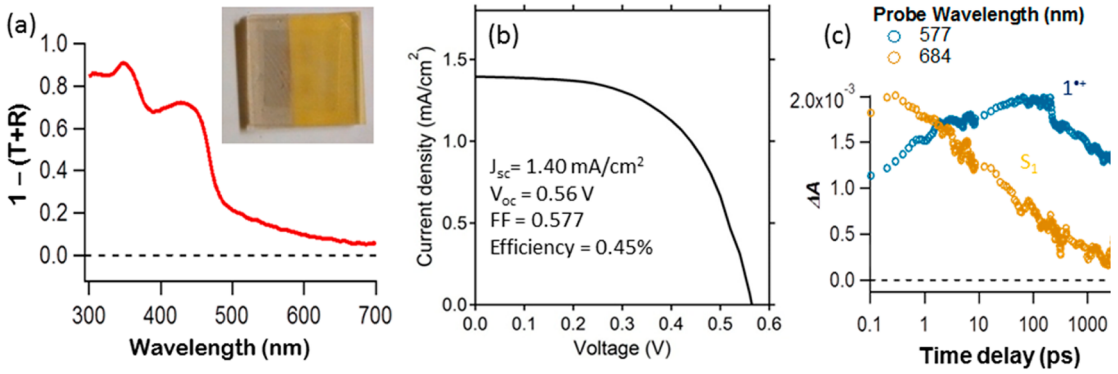

Figure 7. (a) Absorption spectrum of **5** on a mesoporous TiO_2 film. The inset is a photograph of the photoelectrode. (b) $J-V$ curve for a solar cell. (c) Transient absorption showing the rise of the $\mathbf{1}^{\bullet+}$ feature.

in the curve occurs for an average zirconia thickness of 1.5 ± 0.5 nm in both cases. The peaked efficiency curve bears some resemblance to curves found in tetracene/C_{60} or pentacene/C_{60} bilayers, which also exhibit competition between singlet fission and fast charge separation from the singlet state.[31]

The Φ_T value of 100% and the τ_{SF} value of 30 ps in the simulations best match the experimental findings, although other combinations of the yield and rate constant can reproduce the general shape (dashed gray curve in Figure 6b). Further broadening of the experimental curves will likely occur because of variance in true ZrO_2 thicknesses, which was not taken into account in the simulations. Moreover, the significant residual photocurrent at large thicknesses not predicted by the simulations is partially due to the J_{sc} contributed from light absorbed by TiO_2 at wavelengths of <400 nm. For these reasons, deduction of the yield and rate constant of SF by matching photocurrent versus barrier thickness to the kinetic simulations is not definitive.

The collection of ultrafast transient absorption data on photoelectrodes similar to those used for devices was hampered by light scattering in the regions crucial for identifying T_1 and S_1 populations. A bleach feature and broad absorptions are apparent, but the spectra cannot be definitively assigned. Mid-infrared transient absorption experiments (Figure S4 of the Supporting Information) performed with a 4.5 μm probe pulse, expected to probe free electrons in TiO_2, revealed a rise in absorption occurring after 420 nm excitation that increases with a time constant of ∼150 fs. The fast rise is followed by decay on a time scale of a few hundred picoseconds that is likely due to degradation and/or nonlinear recombination. Regardless, it is quite evident that the majority of charge injection events take place from S_1 <1 ps after photoexcitation. Losses in the form of absorbed photons that do not lead to charge injection may result from a fraction of molecules of **1** that become isolated from TiO_2 due to oxidation product aggregation and thus may undergo fluorescence or SF but without the opportunity for charge separation. The formation of lower-energy excimers or charge-transfer states may facilitate fast nonradiative decay that may also reduce the injection yield. With an increasing thickness of ZrO_2, the aforementioned picosecond decay becomes less prominent, which may be due to improved surface state passivation or a slower secondary injection process. The former seems unlikely because the recombination lifetime as measured by IMVS is shorter with more layers of ZrO_2. If we assume the latter, the kinetics with no ZrO_2 barrier can be subtracted from each data set with ZrO_2, and the resulting slow rise can be seen to increase versus ZrO_2 thickness. This rise, attributed to slowed S_1 injection and enhanced T_1 injection, is expected due to the exponential dependence of the injection rate constant on **1**−TiO_2 separation.

To achieve covalent binding of **1** to TiO_2, we synthesized **5**, which is a derivative of **1** that carries a carboxylic acid group. To separate the chromophore from the TiO_2 by a distance that would allow for slowed S_1 injection, we chose a saturated hydrocarbon chain length of ∼6 Å (β = 1.1). Compound **5** has been synthesized in three steps, starting from 1-(4-bromophenyl)-3-phenylisobenzofuran (Scheme 1).[34] In a first step, an ester was obtained using common Sonogashira conditions. Hydrogenation under hydrogen pressure in the presence of palladium black furnished the ester bearing a saturated lateral chain. A final deprotection using aqueous NaOH gave target compound **5**, which sensitized the mesoporous TiO_2 substrates even in the absence of air and remained strongly colored even after acetonitrile rinsing (Figure 7a).

DOI: 10.1021/am506329v
ACS Appl. Mater. Interfaces 2015, 7, 2286−2293

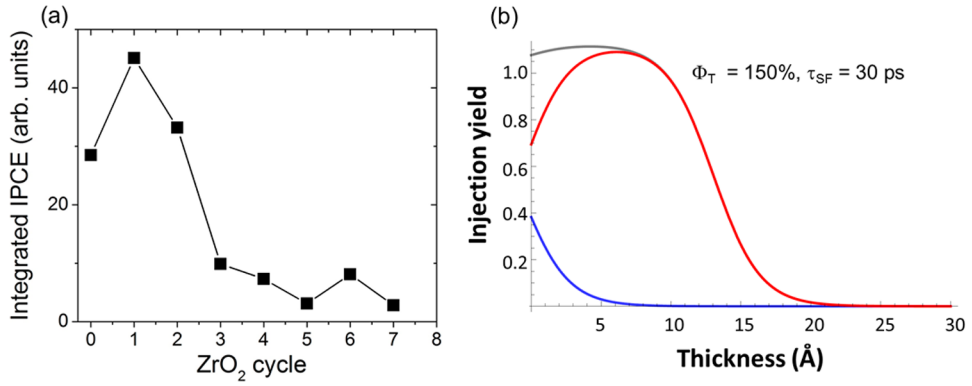

Figure 8. (a) IPCE integrated from 400 to 700 nm for a **5**–TiO_2 solar cell vs ZrO_2 cycle (expected thickness of ~5 Å per cycle). (b) Injection yield vs thickness predicted by kinetic simulation.

The device performance is shown in Figure 7b. The short-circuit photocurrent density is somewhat lower than that of the device made for **1** without the carboxylate linker, and this may indicate that whereas slowed charge injection is caused by the spacer, other factors reduce the overall efficiency. The fill factor is also lower, possibly because of enhanced internal recombination from poorer surface passivation of the electrode. The transient spectra in the visible spectral region show an absorption band that can be assigned to radical cation $\mathbf{1}^{\bullet+}$, which forms upon electron injection (Figure S5 of the Supporting Information).[20] The rise kinetics of this feature do not consist of a single-exponential component with the expected ~30 ps time constant (Figure 7c), which is not surprising given the likely broad distribution of distances between **1** and TiO_2. However, the rise component occurring on a 0.5–10 ps time scale is a strong indication that the saturated hydrocarbon chain has significantly increased the electron injection time from S_1 from the value of <0.2 ps for **1** with no spacer. The radical cation $\mathbf{1}^{\bullet+}$ and the excited singlet kinetics are anticorrelated, as would be expected for injection primarily from S_1.

Solar cells were also fabricated with **5** attached to TiO_2 substrates that had been overcoated with varying thicknesses of ZrO_2. Although the photocurrents produced were considerably smaller than those shown in Figure 6 because of poor dye loading, a rise in light harvesting efficiency (taken either as the IPCE value at 420 nm or the integrated photocurrent from 400 to 700 nm) occurred after one or two layers of ZrO_2 (Figure 8a). This contrasts with the rise occurring after three or four layers of ZrO_2 for **1** without the ~6 Å of saturated linker. Because the injection time is decreased by at least one order of magnitude by the linker, the amount of ZrO_2 needed to slow down the S_1 injection beyond 30 ps is reduced. Kinetic simulations (Figure 8b) assuming a fixed-length saturated chain and variable thickness ZrO_2 barrier confirm the experimental data with a Φ_T of 150%. We note that even without ZrO_2 present, the simulated total injection yield is >1 because of the slowing of S_1 injection by the aliphatic chain. The orientations of **5** and interchromophore geometries at the surface of TiO_2 or ZrO_2 are unknown, and synthesis of more rigid and bipodal linkers is planned, as well as sensitization with a mixture of linker lengths that would potentially allow for more flexibility in forming slip-stacked intermolecular geometries known to be favorable for SF.[35]

CONCLUSIONS

A novel method for detecting the influence of singlet fission on the photocurrent of a solar cell has been demonstrated using the compound 1,3-diphenylisobenzofuran on mesoporous TiO_2 with a varying thickness of zirconia. The injection kinetics, despite containing a broad distribution of lifetimes, supports the kinetic picture in which the insulating zirconia layer reduces the S_1 injection time sufficiently to allow singlet fission to occur, after which triplet injection proceeds. Furthermore, a version of **1** with an aliphatic chain terminated with a carboxylic acid exhibits behavior consistent with an increased barrier to electron injection compared with zirconia and thus a change in the photocurrent versus thickness profile. We find that the dye-sensitized solar cell is a convenient and versatile platform for observing the effect of charge injection after singlet fission, and further efforts with other types of aggregates of **1** may lead to an internal or external quantum efficiency that exceeds 100%.

EXPERIMENTAL PROCEDURES

TiO_2 Photoelectrode. Mesoporous TiO_2 films were screen-printed on a conductive, fluorine-doped tin oxide-coated glass substrate (FTO; TEC8, Hartford, CT) using a paste of 20 nm sized TiO_2 nanoparticles as detailed previously.[36] The average film thickness is approximately 4–8 μm as determined by a surface profiler. Prior to the deposition of the mesoporous TiO_2 film, the FTO substrate was first soaked in a base bath (~5 wt % alcoholic NaOH solution) for 16 h to remove organic contamination and then rinsed sequentially with deionized water and ethanol, followed by blow drying under a flow of N_2. A thin compact TiO_2 layer was deposited on the cleaned FTO substrate by spray pyrolysis[37] of 0.2 M Ti(IV) bis(ethyl acetoacetate)-diisopropoxide in a 1-butanol solution at 450 °C, followed by annealing at 450 °C for 1 h. The printed mesoporous TiO_2 film was annealed at 500 °C for 0.5 h.

ZrO_2 Coating. ZrO_2 coating was performed using previously reported methods.[38,39] The annealed TiO_2 photoelectrodes were cooled to 70 °C, dipped into a 0.04–0.15 M zirconium butanoxide 2-propanol solution at 60 °C for 15 min, and rinsed three times with 2-propanol. The photoelectrodes were then annealed at 500 °C for 0.5 h. Additional cycles of ZrO_2 coating were repeated using the same procedure. Each ZrO_2 coating cycle would introduce a concentration-dependent thickness of ZrO_2, varying from 3 to ~10 Å.

Solar Cell Preparation and Testing. The prepared TiO_2 and ZrO_2/TiO_2 electrodes were immersed in an acetonitrile solution of **1** and kept at room temperature for 24 h in the dark. The counter electrode was prepared by spreading a droplet of 7 mM H_2PtCl_6 in 2-propanol onto the FTO glass followed by annealing at 400 °C for 20 min in air. The TiO_2 working electrode and the Pt-coated counter electrode were then sandwiched together using the 25 μm thick Surlyn (Dupont grade 1702). The electrolyte consisted of 0.8 M HDMII (1-

DOI: 10.1021/am506329v
ACS Appl. Mater. Interfaces 2015, 7, 2286–2293

hexyl-2,3-dimethylimidazolium iodide) and 0.05 M I_2 in methoxypropionitrile.

Spectroscopic Methods. The absorption spectra were characterized by an UV−vis−NIR spectrophotometer (Cary-6000i). The photocurrent−voltage characteristics of dye-sensitized solar cells were measured with a Keithley 2400 source meter under simulated AM 1.5G illumination (100 mW/cm^2; Oriel Sol3A Class AAA Solar Simulator). The uncertainty in J_{sc} due to instrumental variations was <1%, while the device stability contributed no more than 5% to uncertainties (repeated J_{sc} measurement at 30 min intervals). The largest source of error was likely sample-to-sample variations, which could not be systematically tested on the entire set of photoelectrodes, but similar samples fabricated under similar conditions but at different times were tested and found to exhibit an ∼10% difference in J_{sc}. Charge transport and recombination properties of the sensitized cells were measured by intensity-modulated photocurrent and photovoltage spectroscopy as described previously.[28,40] In brief, a 455 nm high-power LED was used to illuminate the sample from the substrate side; it served as both the bias illumination and the small sinusoidally modulated probe beam. IMPS and IMVS measurements were performed at modulation frequencies between 1 mHz and 10 kHz by an SR830 lock-in amplifier. Neutral density filters were used to vary the illumination intensity. The amplitude of the modulated photocurrent density was kept at ≤10% compared to the steady state photocurrent density.

All films intended for transient absorption experiments were sealed under inert conditions using a Surlyn frame and a top glass slide by heating the entire assembly on a hot plate at 90 °C for 5−10 s. Ultrafast transient absorption measurements at low fluence were taken using excitation pulses at 400−450 nm produced by a Coherent Libra regeneratively amplified Ti:sapphire laser with an ∼4 W, 1 kHz, ∼100 fs output at 800 nm; ∼30% of this is directed into a TOPAS-C optical parametric amplifier that is capable of producing wavelengths from 300 to 1600 nm as the excitation source. The excitation beam is attenuated and introduced into an Ultrafast Systems Helios spectrometer. Approximately 10 μJ of the 800 nm Libra output is also directed into the Helios spectrometer, passing along a multipass delay stage that can afford ∼5.8 ns of pump−probe delay, and then focused onto a continuously moving CaF_2 crystal to produce a broadband visible spectrum (300−850 nm), used as the probe beam. The probe is passed through a neutral density filter, where a fraction is picked off to be used as a reference to account for fluctuations in probe intensity. The pump and probe beams are overlapped at the sample with the pump beam having a spot size ∼250 μm in diameter. The excitation is modulated at 500 Hz through an optical chopper to record both pump-on and pump-off spectra. Photodiode arrays are used for detection of both the probe and reference, and the transient signal is calculated via the Helios software. Typical acquisitions scan 5 ns using 200 points with exponential time spacing, using several forward and reverse scans to average while monitoring for sample degradation. Background and chirp corrections were conducted using the Surface Explorer software (Ultrafast Systems), and other data manipulations and plotting were conducted using Igor Pro 6.34A. Midinfrared probe light (4−10 μm) was generated using a TOPAS fitted with a DFG crystal. The experiment was performed in a fashion similar to visible probing except that a HgCdTe array detection system was used, and the entire spectrometer was purged with dry N_2.

Synthesis of 5. *Methyl 6-[4-(3-Phenylisobenzofuran-1-yl)-phenyl]hex-5-ynoate.* 1-(4-Bromophenyl)-3-phenylisobenzofuran (350 mg, 1 mmol), bis(triphenylphosphine) palladium(II) dichloride (43 mg, 0.06 mmol), and copper iodide (8 mg, 0.04 mmol) were charged in a flame-dried round-bottom flask under a positive pressure of argon. Tetrahydrofuran (6 mL) and diethylamine (3 mL) were added under argon. After the mixture had been stirred for 5 min, 5-methyl hexynoate (0.125 mL, 1.1 mmol) was added and the reaction mixture stirred under argon at 40 °C. After 16 h, the reaction mixture was concentrated to dryness and chromatographed (silica gel, CH_2Cl_2, R_f = 0.5). The fractions containing the target compound were concentrated, and 252 mg (64% yield) of yellow solid was obtained with sufficient purity to be engaged in the next step: ^{1}H NMR ($CDCl_3$, 300 MHz) δ 7.98−7.84 (m, 6H), 7.54−7.49 (m, 4H), 7.36−7.29 (m, 1H), 7.11−7.01 (m, 2H), 3.73 (s, 3H), 2.63−2.48 (m, 4H), 2.06−1.90 (m, 2H).

Methyl 6-[4-(3-Phenylisobenzofuran-1-yl)phenyl]hexanoate. Palladium black (80 mg) was added to a suspension of methyl 6-[4-(3-phenylisobenzofuran-1-yl)phenyl]hex-5-ynoate (252 mg, 0.64 mmol) in methanol (10 mL). The reaction mixture was pressurized under 3 atm of H_2 and stirred at room temperature. After 3 h, the reaction mixture was filtered and the filtrate concentrated to dryness and chromatographed (silica gel, 9/1 cyclohexane/ethyl acetate). The light yellow fluorescent band was collected and concentrated to produce 52 mg (23% yield) of yellow solid that was immediately engaged in the next step: ^{1}H NMR (acetone-d_6, 300 MHz) δ 8.11−7.88 (m, 5H), 7.80−7.60 (m, 1H), 7.60−7.47 (t, J = 8.1 Hz, 2H), 7.42−7.25 (m, 3H), 7.17−7.00 (m, 2H), 3.62 (s, 3H), 2.75−2.59 (t, J = 7.4 Hz, 2H), 2.35−2.30 (t, J = 7.4 Hz, 2H), 1.76−1.55 (m, 4H), 1.49−1.36 (m, 2H).

*6-[4-(3-Phenylisobenzofuran-1-yl)phenyl]hexanoic Acid (**5**).* Methyl 6-[4-(3-phenylisobenzofuran-1-yl)phenyl]hexanoate (58 mg, 0.15 mmol) was dissolved in methanol (30 mL), and 0.2 N NaOH (4.5 mL) was added. The reaction mixture was refluxed for 3 h and concentrated to dryness. Water (15 mL) was added to the residue and the mixture acidified with 2 N HCl and then extracted with CH_2Cl_2. The organic phase was concentrated and chromatographed (silica gel, 1/1 hexane/ethyl acetate). The light yellow fluorescent band was collected and concentrated to produce 18 mg (32% yield) of yellow solid: ^{1}H NMR (acetone-d_6, 300 MHz) δ 8.08−7.02 (m, 13H), 2.76−2.59 (m, 2H), 2.39−2.22 (m, 2H), 1.76−1.54 (m, 4H), 1.50−1.33 (m, 2H).

■ ASSOCIATED CONTENT

Ⓢ Supporting Information

Further solar cell results, experiments with conventional dyes, IMPS and IMVS of zirconia-coated electrodes, information about kinetic simulations, further transient absorption results, and zirconia thickness-dependent photocurrents. This material is available free of charge via the Internet at http://pubs.acs.org.

■ AUTHOR INFORMATION

Corresponding Authors

*E-mail: justin.johnson@nrel.gov.
*E-mail: kai.zhu@nrel.gov.

Notes

The authors declare no competing financial interest.

■ ACKNOWLEDGMENTS

This material is based on worked supported by the U.S. Department of Energy (DOE), Office of Basic Energy Sciences, Division of Chemical Sciences, Biosciences, and Geosciences. J.N.S., J.L.R., Y.Z., K.Z., and J.C.J. acknowledge Contract DE-AC36-08GO28308 with NREL, and J.M. and P.I.D. acknowledge DOE Grant DE-SC0007004.

■ REFERENCES

(1) Smith, M.; Michl, J. Singlet Fission. *Chem. Rev.* **2010**, *110*, 6891−6936.
(2) Nozik, A. J.; Beard, M. C.; Luther, J. M.; Law, M.; Ellingson, R. J.; Johnson, J. C. Semiconductor Quantum Dots and Quantum Dot Arrays and Applications of Multiple Exciton Generation to Third-Generation Photovoltaic Solar Cells. *Chem. Rev.* **2010**, *110*, 6873−6890.
(3) Pope, M.; Geacintov, N. E.; Vogel, F. E. Singlet Exciton Fission and Triplet-Triplet Exciton Fusion in Crystalline Tetracene. *Mol. Cryst. Liq. Cryst.* **1969**, *6*, 83−104.
(4) Smith, M. B.; Michl, J. Recent Advances in Singlet Fission. *Annu. Rev. Phys. Chem.* **2013**, *64*, 361−386.

DOI: 10.1021/am506329v
ACS Appl. Mater. Interfaces 2015, 7, 2286−2293

(5) Chan, W. L.; Berkelbach, T. C.; Provorse, M. R.; Monahan, N. R.; Tritsch, J. R.; Hybertsen, M. S.; Reichman, D. R.; Gao, J. L.; Zhu, X. Y. The Quanum Coherent Mechanism for Singlet Fission: Experiment and Theory. *Acc. Chem. Res.* **2013**, *46*, 1321−1329.
(6) Zimmerman, P. M.; Musgrave, C. B.; Head-Gordon, M. A Correlated Electron View of Singlet Fission. *Acc. Chem. Res.* **2013**, *46*, 1339−1347.
(7) Chan, W. L.; Ligges, M.; Jailaubekov, A.; Kaake, L.; Miaja-Avila, L.; Zhu, X. Y. Observing the Multiexciton State in Singlet Fission and Ensuing Ultrafast Multielectron Transfer. *Science* **2011**, *334*, 1541−1545.
(8) Roberts, S. T.; McAnally, R. E.; Mastron, J. N.; Webber, D. H.; Whited, M. T.; Brutchey, R. L.; Thompson, M. E.; Bradforth, S. E. Efficient Singlet Fission Discovered in a Disordered Acene Film. *J. Am. Chem. Soc.* **2012**, *134*, 6388−6400.
(9) Eaton, S. W.; Shoer, L. E.; Karlen, S. D.; Dyar, S. M.; Margulies, E. A.; Veldkamp, B. S.; Ramanan, C.; Hartzler, D. A.; Savikhin, S.; Marks, T. J.; Wasielewski, M. R. Singlet Exciton Fission in Polycrystalline Thin Films of a Slip-Stacked Perylenediimide. *J. Am. Chem. Soc.* **2013**, *135*, 14701−14712.
(10) Akdag, A.; Havlas, Z.; Michl, J. Search for a Small Chromophore with Efficient Singlet Fission: Biradicaloid Heterocycles. *J. Am. Chem. Soc.* **2012**, *134*, 14624−14631.
(11) Ito, S.; Minami, T.; Nakano, M. Diradical Character Based Design for Singlet Fission of Condensed-Ring Systems with 4nπ Electrons. *J. Phys. Chem. C* **2012**, *116*, 19729−19736.
(12) Paci, I.; Johnson, J. C.; Chen, X. D.; Rana, G.; Popovic, D.; David, D. E.; Nozik, A. J.; Ratner, M. A.; Michl, J. Singlet Fission for Dye-Sensitized Solar Cells: Can a Suitable Sensitizer Be Found? *J. Am. Chem. Soc.* **2006**, *128*, 16546−16553.
(13) Zeng, T.; Hoffmann, R.; Ananth, N. Seeking Small Molecules for Singlet Fission: A Heteroatom Substitution Strategy. *J. Am. Chem. Soc.* **2014**, *136*, 12638−12647.
(14) Congreve, D. N.; Lee, J.; Thompson, N. J.; Hontz, E.; Yost, S. R.; Reusswig, P. D.; Bahlke, M. E.; Reineke, S.; Van Voorhis, T.; Baldo, M. A. External Quantum Efficiency above 100% in a Singlet-Exciton-Fission-Based Organic Photovoltaic Cell. *Science* **2013**, *340*, 334−337.
(15) Hanna, M. C.; Nozik, A. J. Solar Conversion Efficiency of Photovoltaic and Photoelectrolysis Cells with Carrier Multiplication Absorbers. *J. Appl. Phys.* **2006**, *100*, 074510.
(16) Lee, J.; Jadhav, P.; Reusswig, P. D.; Yost, S. R.; Thompson, N. J.; Congreve, D. N.; Hontz, E.; Van Voorhis, T.; Baldo, M. A. Singlet Exciton Fission Photovoltaics. *Acc. Chem. Res.* **2013**, *46*, 1300−1311.
(17) Janssen, R. A. J.; Nelson, J. Factors Limiting Device Efficiency in Organic Photovoltaics. *Adv. Mater.* **2013**, *25*, 1847−1858.
(18) Oregan, B.; Gratzel, M. A Low-Cost, High-Efficiency Solar-Cell Based on Dye-Sensitized Colloidal TiO_2 Films. *Nature* **1991**, *353*, 737−740.
(19) Jeong, N. C.; Son, H. J.; Prasittichai, C.; Lee, C. Y.; Jensen, R. A.; Farha, O. K.; Hupp, J. T. Effective Panchromatic Sensitization of Electrochemical Solar Cells: Strategy and Organizational Rules for Spatial Separation of Complementary Light Harvesters on High-Area Photoelectrodes. *J. Am. Chem. Soc.* **2012**, *134*, 19820−19827.
(20) Schwerin, A. F.; Johnson, J. C.; Smith, M. B.; Sreearunothai, P.; Popovic, D.; Cerny, J.; Havlas, Z.; Paci, I.; Akdag, A.; MacLeod, M. K.; Chen, X. D.; David, D. E.; Ratner, M. A.; Miller, J. R.; Nozik, A. J.; Michl, J. Toward Designed Singlet Fission: Electronic States and Photophysics of 1,3-Diphenylisobenzofuran. *J. Phys. Chem. A* **2010**, *114*, 1457−1473.
(21) Johnson, J. C.; Akdag, A.; Zamadar, M.; Chen, X. D.; Schwerin, A. F.; Paci, I.; Smith, M. B.; Havlas, Z.; Miller, J. R.; Ratner, M. A.; Nozik, A. J.; Michl, J. Toward Designed Singlet Fission: Solution Photophysics of Two Indirectly Coupled Covalent Dimers of 1,3-Diphenylisobenzofuran. *J. Phys. Chem. B* **2013**, *117*, 4680−4695.
(22) Johnson, J. C.; Michl, J. In *Advanced Concepts in Photovoltaics*; Nozik, A., Beard, M. C., Conibeer, G., Eds.; Royal Society of Chemistry: London, 2014; Chapter 10, pp 324−344.
(23) Schrauben, J. N.; Ryerson, J. L.; Michl, J.; Johnson, J. C. Mechanism of Singlet Fission in Thin Films of 1,3-Diphenylisobenzofuran. *J. Am. Chem. Soc.* **2014**, *136*, 7363−7373.
(24) Ryerson, J. L.; Schrauben, J. N.; Ferguson, A. J.; Sahoo, S. C.; Naumov, P.; Havlas, Z.; Michl, J.; Nozik, A. J.; Johnson, J. C. Two Thin Film Polymorphs of the Singlet Fission Compound 1,3-Diphenylisobenzofuran. *J. Phys. Chem. C* **2014**, *118*, 12121−12132.
(25) Johnson, J. C.; Nozik, A. J.; Michl, J. High Triplet Yield from Singlet Fission in a Thin Film of 1,3-Diphenylisobenzofuran. *J. Am. Chem. Soc.* **2010**, *132*, 16302−16303.
(26) Howard, J. A.; Mendenhall, G. D. Autoxidation and Photooxidation of 1,3-Diphenylisobenzofuran: Kinetic and Product Study. *Can. J. Chem.* **1975**, *53*, 2199−2201.
(27) Zhang, X. F.; Yang, X. D. Singlet Oxygen Generation and Triplet Excited-State Spectra of Brominated Bodipy. *J. Phys. Chem. B* **2013**, *117*, 5533−5539.
(28) Zhu, K.; Neale, N. R.; Miedaner, A.; Frank, A. J. Enhanced Charge-Collection Efficiencies and Light Scattering in Dye-Sensitized Solar Cells Using Oriented TiO_2 Nanotubes Arrays. *Nano Lett.* **2007**, *7*, 69−74.
(29) Prasittichai, C.; Avila, J. R.; Farha, O. K.; Hupp, J. T. Systematic Modulation of Quantum (Electron) Tunneling Behavior by Atomic Layer Deposition on Nanoparticulate SnO_2 and TiO_2 Photoanodes. *J. Am. Chem. Soc.* **2013**, *135*, 16328−16331.
(30) Lee, S. H. A.; Zhao, Y. X.; Hernandez-Pagan, E. A.; Blasdel, L.; Youngblood, W. J.; Mallouk, T. E. Electron Transfer Kinetics in Water Splitting Dye-Sensitized Solar Cells Based on Core-Shell Oxide Electrodes. *Faraday Discuss.* **2012**, *155*, 165−176.
(31) Yost, S. R.; Lee, J.; Wilson, M. W. B.; Wu, T.; McMahon, D. P.; Parkhurst, R. R.; Thompson, N. J.; Congreve, D. N.; Rao, A.; Johnson, K.; Sfeir, M. Y.; Bawendi, M. G.; Swager, T. M.; Friend, R. H.; Baldo, M. A.; Van Voorhis, T. A Transferable Model for Singlet-Fission Kinetics. *Nat. Chem.* **2014**, *6*, 492−497.
(32) Kallioinen, J.; Benko, G.; Sundstrom, V.; Korppi-Tommola, J. E.; Yartsev, A. P. Electron Transfer from the Singlet and Triplet Excited States of $Ru(dcbpy)_2(NCS)_2$ into Nanocrystalline TiO_2 Thin Films. *J. Phys. Chem. B* **2002**, *106*, 4396−4404.
(33) Feng, X.; Kolomeisky, A. B.; Krylov, A. I. Dissecting the Effect of Morphology on the Rates of Singlet Fission: Insights from Theory. *J. Phys. Chem. C* **2014**, *118*, 19608−19617.
(34) Kuninobu, Y.; Seiki, T.; Kanamaru, S.; Nishina, Y.; Takai, K. Synthesis of Functionalized Pentacenes from Isobenzofurans Derived from C-H Bond Activation. *Org. Lett.* **2010**, *12*, 5287−5289.
(35) Johnson, J. C.; Nozik, A. J.; Michl, J. The Role of Chromophore Coupling in Singlet Fission. *Acc. Chem. Res.* **2013**, *46*, 1290−1299.
(36) Zhao, Y. X.; Zhu, K. Charge Transport and Recombination in Perovskite $(CH_3NH_3)PbI_3$ Sensitized TiO_2 Solar Cells. *J. Phys. Chem. Lett.* **2013**, *4*, 2880−2884.
(37) Cameron, P. J.; Peter, L. M. Characterization of Titanium Dioxide Blocking Layers in Dye-Sensitized Nanocrystalline Solar Cells. *J. Phys. Chem. B* **2003**, *107*, 14394−14400.
(38) Palomares, E.; Clifford, J. N.; Haque, S. A.; Lutz, T.; Durrant, J. R. Control of Charge Recombination Dynamics in Dye Sensitized Solar Cells by the Use of Conformally Deposited Metal Oxide Blocking Layers. *J. Am. Chem. Soc.* **2003**, *125*, 475−482.
(39) Menzies, D. B.; Dai, Q.; Bourgeois, L.; Caruso, R. A.; Cheng, Y. B.; Simon, G. P.; Spiccia, L. Modification of Mesoporous TiO_2 Electrodes by Surface Treatment with Titanium(IV), Indium(III) and Zirconium(IV) Oxide Precursors: Preparation, Characterization and Photovoltaic Performance in Dye-Sensitized Nanocrystalline Solar Cells. *Nanotechnology* **2007**, *18*, 125608.
(40) Schlichthorl, G.; Huang, S. Y.; Sprague, J.; Frank, A. J. Band Edge Movement and Recombination Kinetics in Dye-Sensitized Nanocrystalline TiO_2 Solar Cells: A Study by Intensity Modulated Photovoltage Spectroscopy. *J. Phys. Chem. B* **1997**, *101*, 8141−8155.

DOI: 10.1021/am506329v
ACS Appl. Mater. Interfaces 2015, 7, 2286−2293